Ultrasound Modulated Droplet Lasers

Xuzhou Li,[†,‡,∥] Yu Qin,[†,§,∥] Xiaotian Tan,[†] Yu-Cheng Chen,[†,⊥] Qiushu Chen,[†] Wei-Hung Weng,[#] Xueding Wang,*[,†] and Xudong Fan*[,†] ⬚

[†]Department of Biomedical Engineering, University of Michigan 1101 Beal Avenue, Ann Arbor, Michigan 48109, United States

[‡]Department of Mechanical Engineering, University of Michigan 2350 Hayward Street, Ann Arbor, Michigan 48109, United States,

[§]Institute of Acoustic, School of Physics Science and Engineering, Tongji University, Shanghai 200092, People's Republic of China

[⊥]School of Electrical and Electronic Engineering, Nanyang Technological University, 50 Nanyang Avenue, 639798, Singapore

[#]Computer Science and Artificial Intelligence Laboratory, Massachusetts Institute of Technology, 32 Vassar Street, Cambridge, Massachusetts 02139, United States

Ⓢ Supporting Information

ABSTRACT: We demonstrated the ultrasound modulated droplet lasers, in which the laser intensity from whispering gallery mode (WGM) of oil droplets can be reversibly enhanced up to 20-fold when the ultrasound pressure is beyond a certain threshold. The lasing enhancement was investigated with various ultrasound frequencies and pressures. Furthermore, the ultrasound modulation of the laser output was achieved by controlling the ultrasound pressure, the duty cycle, and the frequency of ultrasound bursts. Its potential application was explored via the study on a human whole blood vessel phantom. A theoretical analysis was also conducted, showing that the laser emission enhancement results from the directional emission from a deformed cavity under ultrasound pressure. Our studies reveal the unique capabilities of ultrasound modulated droplet lasers, which could lead to the development of laser emission-based microscopy for deep tissue imaging with high spatial resolution and detection sensitivity that may overcome the long-standing drawback of traditional fluorescence imaging.

**KEYWORDS:** microlasers, droplets, whispering gallery mode, ultrasound, remote modulation
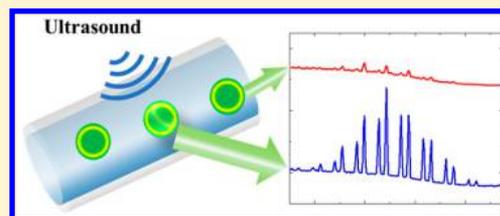
Fluorescence imaging is one of the most commonly used technologies in biomedical applications. When applied to biological tissues beyond the surface, the spatial resolution and sensitivity of fluorescence imaging are degraded, which is due mainly to the overwhelming optical scattering in the tissues and also affected by the background autofluorescence.[1−4] To date, breaking the optical diffusion limit while maintaining the high signal-to-noise ratio (SNR) in fluorescence imaging still remains challenging. On the other hand, ultrasound (US) imaging, owing to the much lower scattering of ultrasound wave in biological tissues, can keep its spatial resolution in deep tissues much better than fluorescence imaging. Therefore, high frequency US is not only employed for imaging,[5−7] but also adapted to treatment such as tumor therapy,[8−10] drug releasing,[11,12] and nerve stimulation.[13−15] Recently, US modulated fluorescence imaging[16,17] has been explored, aiming to improve fluorescence imaging by leveraging the advantages of US in spatial resolution and tissue penetration. In this technique, US wave at a certain frequency is focused in a scattering medium (such as an optically scattering biological tissue), changing the scattering property in the medium thus modulating the photons transmitting through the US modulated area. When building an image from the medium, only the modulated photons carrying the US frequency will be used while the nonmodulated photons will be filtered out. Although holding the potential to improve the spatial resolution of optical imaging, this method suffers from a low signal-to-noise ratio (SNR) resulting from the limited modulation depth, which is defined as the modulated photons over the total photons detected. In an alternative method of US modulated optical imaging, microbubbles labeled with fluorophores and quenchers were used.[18,19] The volume of a microbubble is changed under the US pressure wave, leading to the emergence of fluorescence due to the increased distance between the fluorophores and the quenchers. Since this method still relies on the detection of fluorescence, which is weak in intensity and broad in spectrum, its SNR and spatial resolution are still limited.

In contrast to fluorescence-based detection and imaging, laser emission-based detection and imaging has recently emerged as a novel technology in biomedical research. Compared to fluorescence, laser emission has strong intensity and extremely narrow line width, which leads to significantly improved SNR, imaging contrast, and sensitivity in sensing biological changes.[20−22] Previously, laser emission has been used in ultrasensitive molecule detection[23−25] and cancer diagnosis.[26−29] Additionally, micron- and submicron-sized lasers have been implanted into cells, biological tissues, and
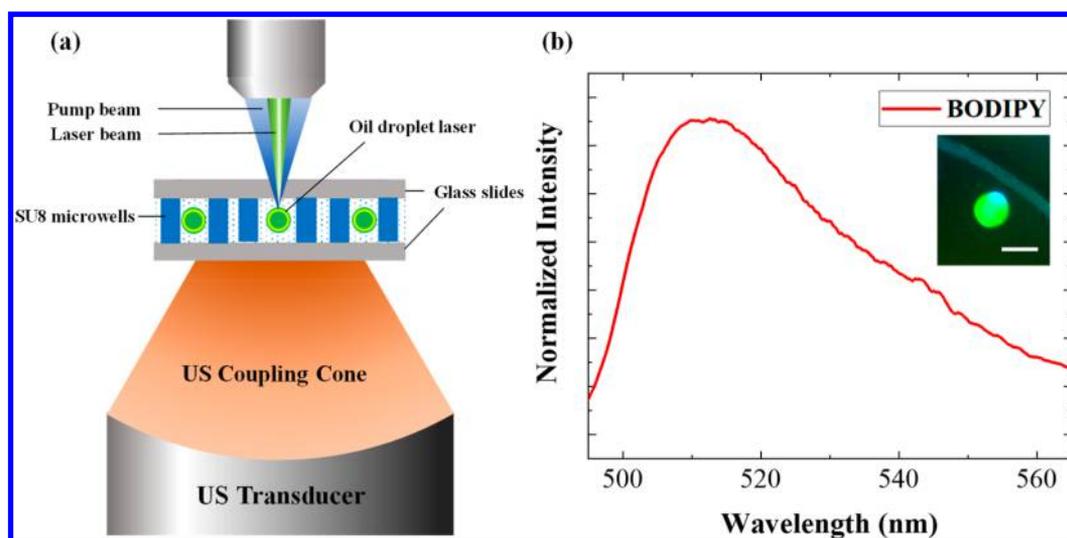
Figure 1. (a) Schematic of the optical and ultrasound (US) setup, in which the oil droplets were trapped inside microwells. The oil droplets doped with BODIPY were excited by a pulsed diode laser (pulse width = 2 ns; wavelength = 473 nm), whereas a focused US beam transmitted through the coupling medium. (b) Fluorescence spectrum of a single oil droplet in the microwell below the lasing threshold. Inset is a CCD image of the droplet. Scale bar: 50 μm.
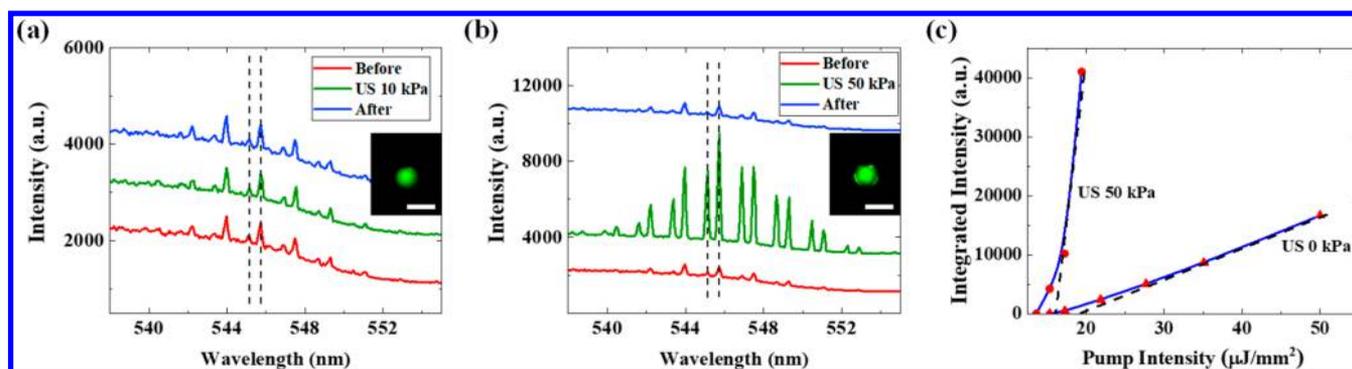
Figure 2. Lasing enhancement with exposure to ultrasound. The same 45 μm diameter oil droplet laser was investigated and the same ultrasound (US) frequency of 500 kHz was applied in (a)−(c). (a) Lasing spectra of the oil droplet laser before, during, and after applying US pressure of 10 kPa. Inset is a CCD image of the droplet laser without US. (b) Lasing spectra of the oil droplet laser before, during, and after applying US pressure of 50 kPa. Inset is a CCD image of the droplet laser with US. All curves in a and b were obtained under the same pump energy density of 35 μJ/mm². Curves in (a) and (b) are vertically shifted for clarity. Dashed lines in (a) and (b) are guides for better observation of the lasing wavelength. Scale bars in (a) and (b): 50 μm. (c) Laser output integrated over the spectral range of 540−560 nm as a function of the pump energy density. The measurements with US (50 kPa) and without US (0 kPa) exposure are compared. The dashed lines are the linear fit above the respective lasing thresholds under US pressure of 50 and 0 kPa. With the exposure to 50 kPa ultrasound, the lasing threshold is reduced from 19 to 11 μJ/mm².

live animals to track cells and detect subtle biological changes.[30−33]

In this study, we explored, for the first time, the US modulated microsized lasers, which, if feasible, could leverage the deep tissue penetration and the high resolution of US imaging and the high SNR, imaging contrast, and sensitivity of laser emission. As an important step toward the US modulated laser emission-based microscopy, we first demonstrated the US modulated microdroplet lasers (Figure 1a), in which the laser emission intensity from the whispering gallery mode (WGM) of an oil droplet laser can be enhanced up to 20-fold when the US pressure reaches a certain threshold. This enhancement in laser emission intensity is reversible when the US is turned off. The lasing enhancement under different US frequencies ranging from 500 kHz to 10 MHz was investigated. Furthermore, the US modulation of the laser output was achieved by controlling the US pressure, the duty cycle, and the modulation frequency. Finally, we explored a potential

application of the US modulated droplet lasing in biology and medicine using phantoms vessels containing human whole blood. A theoretical analysis was also conducted to explain the mechanism of the US modulated droplet lasers.

◼ RESULTS

Lasing Enhancement with Ultrasound. Throughout the experiments, the microdroplets were prepared with a standard oil-in-water dispersion procedure.[34] The lipophilic fluorescence dye, BODIPY, was dissolved in biocompatible and easy-to-obtain corn oil (refractive index RI = 1.46) (Figure 1b). Then, the oil doped with dye was diluted and mixed with surfactant solution until it was dispersed uniformly. Under the effect of surface tension, microdroplets had a spherical shape of 30−50 μm in diameter. Following this, microdroplets were loaded into microwells (Figure 1a and the inset of Figure 1b). In this study, a confocal optical setup was utilized to pump and collect laser emission (Figure 1a). A focused US transducer
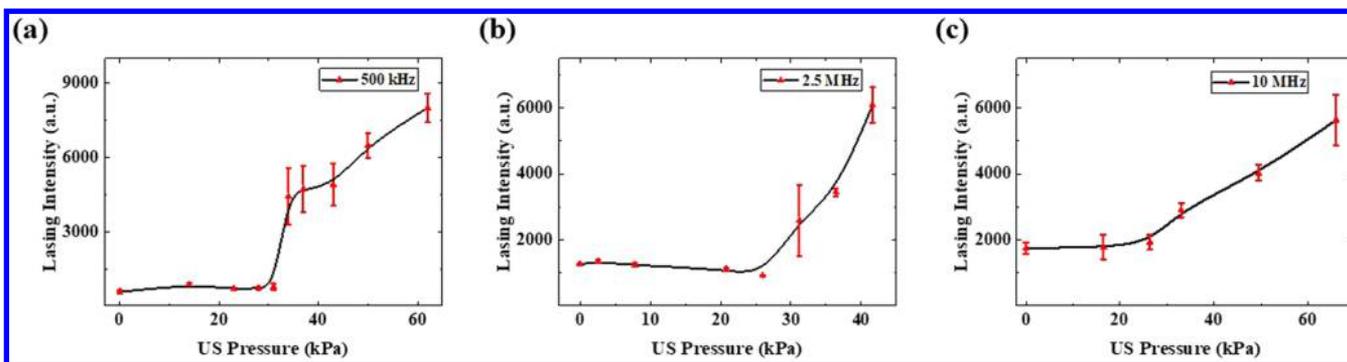
Figure 3. Lasing enhancement with different ultrasound (US) frequencies. (a−c) Lasing intensity as a function of US pressure for US frequency of 500 kHz, 2.5 MHz, and 10 MHz, respectively. All lasing intensities were extracted from the spectra collected under a pump energy density of 40 μJ/mm^2 and an integration time of 1 s. Error bars were obtained with five measurements. Three different 50 μm droplet lasers were investigated respectively in (a)−(c).

was placed at the bottom of the microwell chip and the US beam was focused on the microdroplet via the coupling gel. More details of the setup can be found in the Methods section.

Initially, the lasing spectra of the microdroplet laser were studied under a relatively low US pressure (10 kPa at 500 kHz). During the measurements, the microdroplet lasers were trapped and observed at the same position and with a constant pump energy density of 35 μJ/mm^2. To demonstrate the effect of US, the lasing spectra of the microdroplet laser were recorded before, during, and after continuous US exposure (Figure 2a). Obviously, neither the lasing intensity nor the spectral peak position changed with the "low" US pressure, suggesting that small US disturbance does not affect droplet lasing behavior. In contrast, with a stronger US pressure (50 kPa at 500 kHz), significant enhancement (~20 times) in lasing intensity was observed when the US was turned on (Figure 2b). In particular, strong lasing emission emerges from the rim of the droplet (see the inset of Figure 2b). Furthermore, the enhancement is reversible, that is, the lasing intensity falls back to the normal level when the US was turned off. During the US lasing enhancement, the lasing modes and their spectral positions remained the same (within the spectrometer resolution), indicating that the US, at the given pressure, did not cause any significant change in the shape and size of the oil microdroplets (see more discussion in Supporting Information). In Figure 2c, we investigated the microdroplet lasing threshold with and without the exposure to the US pressure. It was found that the lasing threshold was reduced from 19 to 11 μJ/mm^2 with a 10× increase in the intensity efficiency (the slope of the laser output) when the microdroplet was exposed to the US pressure of 50 kPa.

We further investigated the relationship between the microdroplet lasing intensity and the US frequencies, as the result shown in Figure 3. All the lasing spectra were acquired with the same integration time of 1 s under the fixed pump energy density of 40 μJ/mm^2. Focused ultrasound transducers worked at various frequencies (500 kHz, 2.5 MHz, and 10 MHz, respectively) were utilized to generate continuous US that was applied to microdroplet lasers. We noticed a pressure threshold around 30 kPa for all the three US frequencies. Below the pressure threshold, no enhancement in laser intensity was observed (see also Figure 2a). While above the pressure threshold, the enhancement became linearly proportional to the US pressure. In addition, it seems that the US with lower frequency led to higher enhancement, as

demonstrated by the steeper slope above the pressure threshold in Figure 3a compared to those in Figure 3b,c.

The phenomena observed above, including the lasing intensity enhancement and the ultrasound threshold behavior, can be understood in the framework of directional emission from an asymmetric resonator cavity (ARC).[35−39] In the absence of US, the droplet maintains a nearly perfect spherical shape and the lasing output is weak and isotropic. In the focused ultrasound field, the droplet is steadily deformed to become ellipsoidal by the second-order acoustic radiation force.[40] The quantitative estimation of the acoustic radiation force and the corresponding deformation of the droplet are included in the Supporting Information. With a relatively low acoustic pressure (and hence a low acoustic radiation force), the deformation of the droplet is insignificant, and the weak, isotropic lasing emission is preserved. With the increased acoustic pressure (and hence the increased acoustic radiation force), the smoothly deformed droplet breaks the spherical symmetry of the WGM cavity and the ray dynamics becomes partially chaotic, leading to high power directional laser emission (or chaos-assisted tunneling). Such enhancement in the laser emission directionality, laser output, and laser output efficiency, as well as reduction in the lasing threshold, were previously observed in oscillatory droplets falling in the air and solid disks fabricated on a chip,[35,41,42] but have never been studied under the influence of US. Usually, due to the relatively large refractive index contrast between those WGM cavities and the surrounding media, a relatively large deformation threshold (e.g., 5%) is needed to have directional emission.[35] However, in our case, the refractive index contrast between the oil and water is only 1.1, and therefore, directional emission can be achieved with a smaller deformation. Based on the ultrasound threshold in Figure 3 and the theoretical analysis in Figure S1b, we estimated that even only 0.1% deformation is sufficient to cause the directional emission. For biomedical applications, a low deformation threshold is desirable since low US intensity is needed to modulate droplet lasers.

To further confirm the mechanism of the enhanced lasing emission described above, we conducted two groups of control experiments. First, we studied the fluorescence intensity from the microdroplet of the similar size (~50 μm in diameter) doped with the same concentration of BODIPY (Figure S2). No difference in fluorescence intensity was observed between the strong US pressure (50 kPa at 500 kHz) and no US
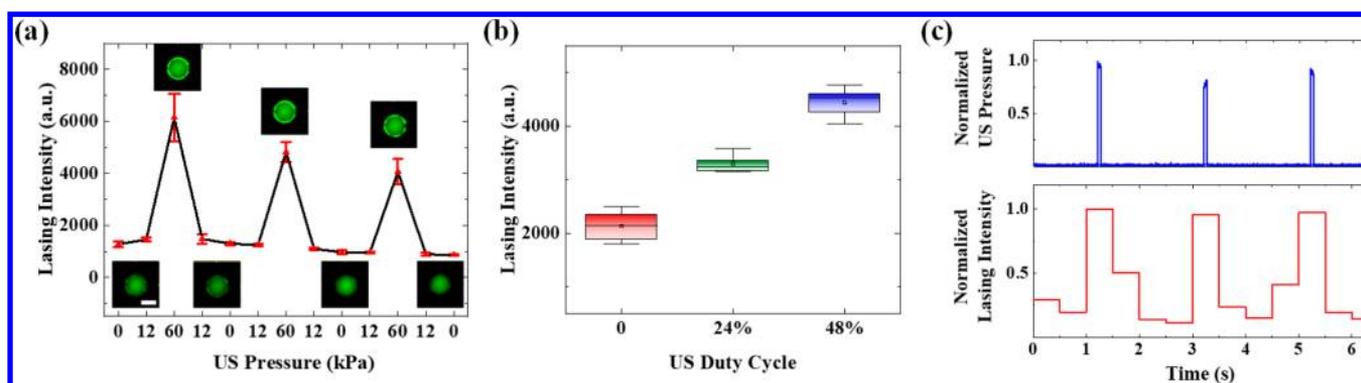
Figure 4. Modulating laser by ultrasound (US). (a) Observation of laser intensities over multiple 500 kHz US pressure cycles (0 → 12 kPa → 60 kPa → 12 kPa → 0). Insets: CCD images of the oil droplet at ground states and lasing enhancement states. The overall downward trend of lasing intensity was caused by the photobleaching effect. Error bars were obtained with 5 measurements. Scale bar: 25 μm. (b) Lasing intensity modulated by the duty cycle of 500 kHz US at 50 kPa. When the US duty cycle increases, lasing output increases accordingly. All lasing intensities in (a) and (b) were extracted from the spectra collected under a pump energy density of 40 μJ/mm^2 and an integration time of 1 s. (c) Lasing emission enhanced by short US bursts (500 kHz, 60 kPa, 60 ms burst duration, 0.5 Hz repetition frequency). The top (blue) curve is US driving signal acquired by an oscilloscope. The bottom (red) curve is extracted from a series of spectra under a pump energy density of 40 μJ/mm^2 and an integration time of 0.5 s. The repetition rate of the pump is 20 Hz, which ensures that there is at least one pump during the US burst.
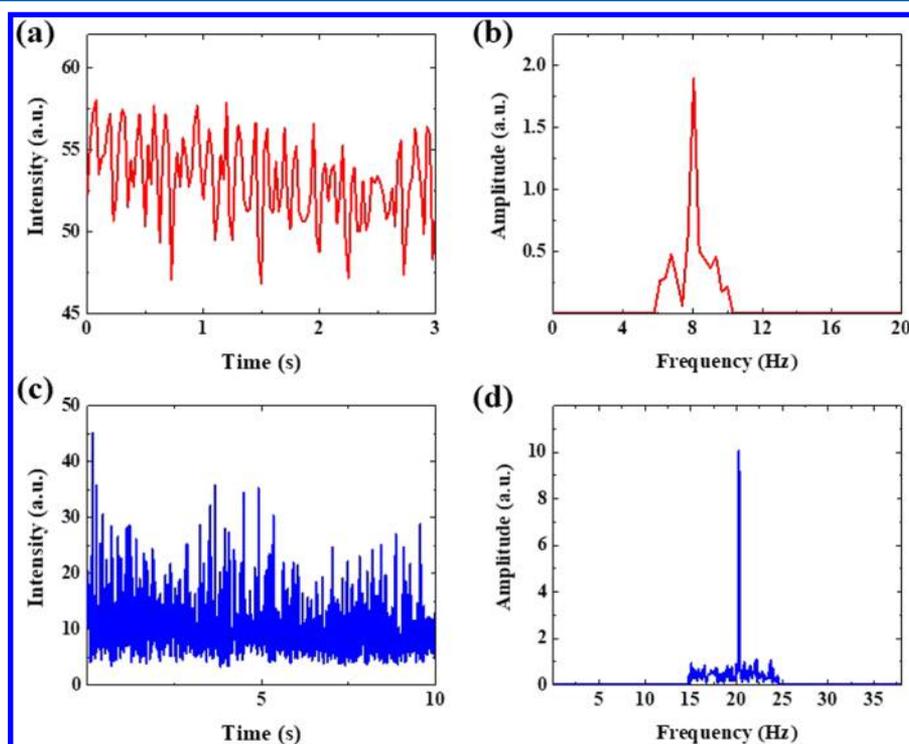

Figure 5. Lasing emission modulated temporally by ultrasound (US). (a) Lasing intensity recorded in the time domain modulated by US bursts (500 kHz, 60 kPa, 30 ms burst duration, 8 Hz repetition frequency). The lasing intensity under a pump energy density of 50 μJ/mm^2 with a pulse repetition rate of 40 Hz was recorded from a CCD with 40 fps. (b) Frequency spectrum when applying FFT to the lasing intensity in (a) with a bandpass filter (6−8 Hz). A peak at the 8-Hz modulation frequency can be noted. (c) Lasing intensity recorded in the time domain modulated by US bursts (500 kHz, 60 kPa, 15 ms burst duration, 20 Hz repetition frequency). The lasing intensity under a pump energy density of 50 μJ/mm^2 with a pulse repetition rate of 80 Hz was recorded from a CCD with 80 fps. (d) Frequency spectrum when applying FFT to the lasing intensity in (c) with a bandpass filter (15−25 Hz). There is a notable 20 Hz modulated component in the spectrum.

pressure (0 kPa), indicating that US has no effect on the fluorescence efficiency of the dye molecules. Second, in Figure S3 we performed the same US enhanced lasing emission on 10 μm diameter polystyrene beads doped with fluorescence dye, FITC. When pumped at 485 nm, lasing emission from the beads was clearly observed. However, even in the presence of a strong US pressure (50 kPa at 500 kHz), the lasing intensity remains virtually unchanged due to the high Young's modulus

(3 GPa) of polystyrene and hence the negligible bead deformation.

Microdroplet Lasers Modulated by Ultrasound. *Control of Droplet Laser Emission by Ultrasound.* Figure 4a shows the capability to noninvasively modulate the microdroplet laser emission by changing the US intensity. In particular, a 500 kHz focused US transducer was used to produce multiple cycles of pressure (0 → 12 kPa → 60 kPa →
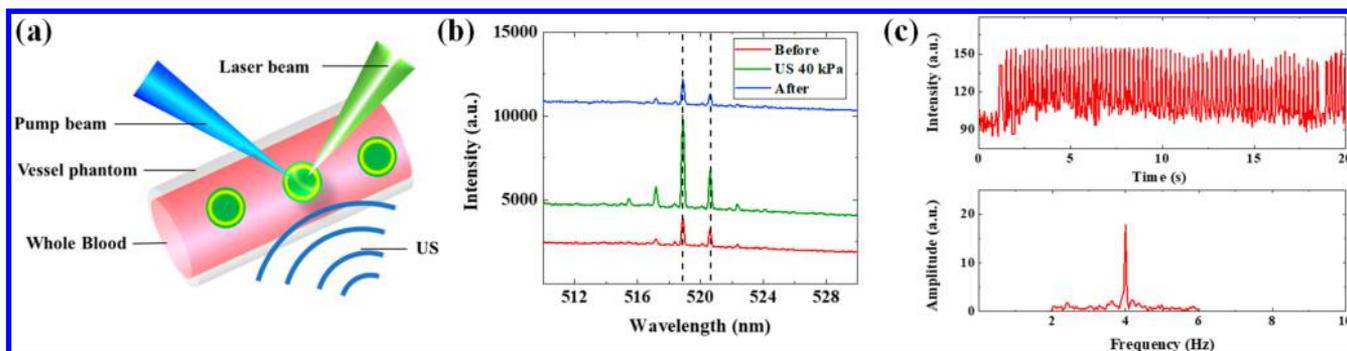
Figure 6. Ultrasound (US) modulated oil droplet lasers in blood. (a) Schematic of the experiment. (b) Lasing spectra of an oil droplet laser mixed with human whole blood and loaded into a capillary before, during, and after applying US pressure (40 kPa at 500 kHz). All curves were obtained under the same pump energy density of 50 μJ/mm^2 with a pulse repetition rate of 20 Hz. Curves are vertically shifted for clarity. (c) (Top) Lasing intensity collected from the whole blood in the time domain with US bursts (500 kHz, 60 kPa, 60 ms burst duration, 4 Hz repetition frequency). The lasing intensity was recorded from a CCD with 20 fps under a pump energy density of 70 μJ/mm^2 with a pulse repetition rate of 20 Hz. (Bottom) Corresponding frequency spectrum of the lasing intensity processed with a bandpass FFT filter (2−6 Hz). There is a notable 4 Hz component in the spectrum.

12 kPa → 0). Every time when a strong US pressure of 60 kPa was applied, significant lasing enhancement of 4−6-fold could be observed compared to the laser emission at US pressure of 0 and 12 kPa. In addition to the US intensity, the laser emission can also be controlled by the US duty cycle. Figure 4b presents the laser emission intensity with 0%, 24%, and 48% duty cycle under the same US pressure (50 kPa at 500 kHz). With the increased duty cycle, the lasing intensity increases linearly. Finally, we demonstrate the laser emission enhancement by short US bursts. A series of US bursts (500 kHz, 60 kPa, 60 ms burst duration) was utilized to trigger the enhanced microdroplet laser emission with a repetition frequency of 0.5 Hz. The laser emission was collected with an exposure time of 0.5 s. From the synchronized US pressure and laser intensity curves in Figure 4c, it can be seen that the lasing intensity follows the US burst at the same repetition frequency (see also the video in the Supporting Information).

Temporal Modulation of Droplet Laser Emission by Ultrasound. The ability to temporally modulate the laser emission is the key to significantly improving the SNR. This becomes even more critical when applying the microdroplet laser for sensing and imaging in deep tissues. First, a series of short US bursts (500 kHz, 60 kPa, 30 ms burst duration) with a repetition frequency of 8 Hz was applied to the microdroplet laser. A CCD camera was used to continuously record the laser output intensity. The pump laser was set at 40 Hz with an energy density of 50 μJ/mm^2 to match the image sampling rate of 40 fps. Figure 5a presents the raw intensity curve as a function of time extracted from the recorded images. Figure 5b shows the frequency domain analysis of the signal in Figure 5a with a bandpass (6−10 Hz) FFT digital filter. A distinct 8 Hz component in the frequency spectrum is observed corresponding to the 8 Hz US bursts. Then, a series of short US bursts (500 kHz, 60 kPa, 15 ms burst duration) with a repetition frequency of 20 Hz was applied to the microdroplet laser. Similarly, the pump laser was set at 80 Hz with an energy density of 50 μJ/mm^2 to match the image sampling rate of 80 fps. Figure 5c presents the raw intensity curve as a function of time extracted from the recorded images. By applying a bandpass FFT digital filter (15−25 Hz), a 20 Hz modulated frequency component in laser output can be seen in Figure 5d with an SNR of approximately 30.

Ultrasound-Modulated Oil Droplet Lasers in Blood. To demonstrate the potential applications of the US modulated droplet laser to biological tissues, in Figure 6a we used a glass capillary embedded 1 mm in an optical scattering gel to simulate a blood vessel. The oil droplets were mixed with human whole blood and injected into the capillary. Initially, a continuous US pressure (40 kPa at 500 kHz) was focused on the blood vessel phantom, and enhanced lasing intensity was observed. The enhancement was reversible after turning the US off (Figure 6b). This result verifies that the US lasing enhancement persists even when the droplets are surrounded by whole blood. Next, a series of short US bursts (500 kHz, 60 kPa, 60 ms burst duration) at 4 Hz repetition frequency was used to modulate the droplet laser. The lasing emission was collected by a CCD camera with 20 fps, as the result shown in Figure 6c. After applying a bandpass FFT digital filter of 2−6 Hz, the modulation component at 4 Hz can be easily extracted with a high SNR of 25, as shown in Figure 6c.

■ DISCUSSION

In this study, we demonstrated the first "ultrasound modulated droplet laser" utilizing biocompatible microdroplet lasers and low intensity focused ultrasound transducers. First of all, lasing intensity enhancement was observed and investigated under various US frequencies and continuous pressure. Besides, we explored modulating droplet laser output with US duty cycle and short bursts. Moreover, the temporal modulation of laser output was achieved with a series of US short bursts at a specific frequency and frequency domain analysis. In addition, we validated that the ultrasound modulated droplet lasers could work well in biological samples such as vessels containing human whole blood. In all the experiments, the pump energy density was orders of magnitude lower than the level that may cause damage to cells or tissues, demonstrating that the US modulated droplet lasers could be developed into noninvasive imaging and sensing technologies.

Our study provides a possible solution to break the optical diffusion limit and significantly improves the spatial resolution, sensitivity, and imaging depth, which overcomes the long-standing drawbacks of conventional fluorescence techniques. By combining the advantages of US imaging, including deep tissue penetration and high spatial resolution with the advantages of laser emission, including high SNR, imaging

contrast, and sensitivity, the ultrasound modulated droplet laser presented in this work opens a door to a new generation of laser emission microscopy for imaging and sensing in deep biological tissues. Below we discuss several scenarios and possible methods to exploit US modulated droplet lasers. By conjugating the droplet lasers with targeted cells, imaging and tracking of cellular dynamics could be achieved in vivo in subsurface tissues. Without targeting any biological entities, the droplet lasers injected into the circulatory system such as blood vessels can also work as a blood pool agent to achieve high-resolution laser emission imaging of the vasculature, as well as flow dynamics in biological samples. Besides potential contributions to biology and medicine, the method described in this work provides a new platform to tune the cavity shape and size remotely, noninvasively, and continuously by ultrasound, which is important for fundamental research and the development of novel photonic devices.

METHODS

Generation of Microdroplets. BODIPY used in this study was purchased from ThermoFisher (Catalog #D3921). Detergent and dichloromethane were purchased from Sigma-Aldrich. Corn oil was purchased from a local supplier. Microdroplets were generated by the standard oil-in-water dispersion procedure.[34] 15 μL of corn oil doped with BODIPY was mixed with 985 μL of diluted detergent and the mixture was shaken for 5 min until the oil was dispersed uniformly in the solvent. In experiments, we diluted the microdroplet solution prepared above 25× in order to easily observe single droplets.

Microwells and Capillaries. A 3 × 3 array of microwells 50 μm in depth and 1 mm in diameter were fabricated in a biocompatible negative photoresist SU-8 on the surface of a 1″ × 1″ glass slide using standard soft lithography. The mirrors were first cleaned by solvent ultrasonication (sonicated in acetone, ethanol, and deionized water sequentially) and oxygen plasma treatment. Then, they were dehydrated at 150 °C for 15 min right before a 50 μm thick SU-8 2025 (MicroChem Corp., U.S.A.) layer was spin-coated on the top of the mirrors. After soft-baking the SU-8-coated mirrors for 3 min at 65 °C and 8 min at 95 °C, a contact lithography tool Karl Suss MA 45S was used to UV-expose the mirrors through a mask. The exposed mirrors were subsequently subjected to postexposure baking at 65 °C for 1 min and 95 °C for 6 min, followed by 8 min of development. After rinsing and drying, the microwell array was further hard baked at 150 °C for 10 min and treated with oxygen plasma to improve hydrophilicity. Before experimental measurement, the microdroplet solution was dripped into the microwells, which were then covered with a glass slide.

The glass capillary, which was used to simulate a blood vessel, was purchased from Thomas Scientific. It had a diameter of 700 μm and a wall thickness of 100 μm. To start with, the microdroplet solution was diluted 20× and mixed with human whole blood. Then the mixture was injected into the capillary, which was later sealed with UV curable epoxy (NOA 81). Finally, the capillary loaded with the sample was submerged 1 mm into US coupling gel.

Optical and Ultrasound Setup. A typical confocal setup was used to excite the oil droplet lasers and collect emission light. (Figure 1a). In this work, a pulsed diode laser (pulse width: 2 ns, tunable repetition rate from 20 to 799 Hz) at 473 nm was loosely focused through a 20 mm focal length cylindrical lens to excite the oil microdroplets in microwells or capillaries. In the control experiments, a pulsed OPO laser (pulse width: 5 ns, repetition rate: 20 Hz) with 485 nm was applied to excite polystyrene beads doped with FITC. The pump intensity was controlled by a continuously variable neutral density filter. The emission light was collected through the same lens and sent to a spectrometer (Horiba iHR550, spectral resolution ∼0.2 nm) for further analysis. For ultrasound modulation, focused ultrasound transducers with 500 kHz, 2.5 MHz, 10 MHz central frequency (500 kHz: H107, Sonic Concepts, Bothell, WA; 2.5 MHz: V307, Olympus Inc.; 10 MHz, V322, Olympus, Inc.) were driven by a function generator (Stanford Research Systems DS345) and a power amplifier (37 dB, custom design) to generate the desired US signals. A commercial calibrated hydrophone (ONDA HNC-1500) was used to measure the applied US pressure during the experiments at the focus of the ultrasound field.

ASSOCIATED CONTENT

ⓢ Supporting Information

The Supporting Information is available free of charge on the ACS Publications website at DOI: 10.1021/acsphotonics.8b01537.

> Illustration of the deformation model and theoretical calculation of the radius deformation ratio of the droplet as a function of the ultrasound are given in Figure S1. Fluorescence intensity comparison of an oil droplet doped with BODIPY with and without applying ultrasound pressure given in Figure S2. Lasing intensity comparison of a polystyrene bead doped with FITC with and without applying ultrasound pressure given in Figure S3 (PDF).

> A video of the droplet laser modulated by ultrasound short bursts at 4 Hz demonstrated in Media S1 (AVI).

AUTHOR INFORMATION

Corresponding Authors
*E-mail: xdwang@umich.edu.
*E-mail: xsfan@umich.edu.

ORCID 🄾
Xudong Fan: 0000-0003-0149-1326

Author Contributions
∥These authors contributed equally to this work.

Notes
The authors declare no competing financial interest.

REFERENCES

(1) Andersson-Engels, S.; Klinteberg, C.; Svanberg, K.; Svanberg, S. In vivo fluorescence imaging fosr tissue diagnostics. *Phys. Med. Biol.* **1997**, *42*, 815−824.

(2) Ntziachristos, V.; Bremer, C.; Weissleder, R. Fluorescence imaging with near-infrared light: new technological advances that enable in vivo molecular imaging. *Eur. Radiol.* **2003**, *13*, 195−208.

(3) Bashkatov, A. N.; Genina, E. A.; Kochubey, V. I.; Tuchin, V. V. Optical properties of human skin, subcutaneous and mucous tissues in

the wavelength range from 400 to 2000 nm. *J. Phys. D: Appl. Phys.* **2005**, *38*, 2543−2555.

(4) Clendenon, S. G.; Young, P. A.; Ferkowicz, M.; Phillips, C.; Dunn, K. W. Deep tissue fluorescent imaging in scattering specimens using confocal microscopy. *Microsc. Microanal.* **2011**, *17*, 614−617.

(5) Kimmey, M. B.; Martin, R. W.; Haggitt, R. C.; Wang, K. Y.; Franklin, D. W.; Silverstein, F. E. Histologic correlates of gastrointestinal ultrasound images. *Gastroenterology* **1989**, *96*, 433−441.

(6) Tranquart, F.; Grenier, N.; Eder, V.; Pourcelot, L. Clinical use of ultrasound tissue harmonic imaging. *Ultrasound Med. Biol.* **1999**, *25*, 889−894.

(7) Errico, C.; Pierre, J.; Pezet, S.; Desailly, Y.; Lenkei, Z.; Couture, O.; Tanter, M. Ultrafast ultrasound localization microscopy for deep super-resolution vascular imaging. *Nature* **2015**, *527*, 499−502.

(8) Orsi, F.; Zhang, L.; Arnone, P.; Orgera, G.; Bonomo, G.; Della Vigna, P.; Monfardini, L.; Zhou, K.; Chen, W.; Wang, Z.; Veronesi, U. High-intensity focused ultrasound ablation: Effective and safe therapy for solid tumors in difficult locations. *AJR, Am. J. Roentgenol.* **2010**, *195*, 245−252.

(9) Zhou, Y. F. High intensity focused ultrasound in clinical tumor ablation. *World J. Clin. Oncol.* **2011**, *2*, 8−27.

(10) Al-Bataineh, O.; Jenne, J.; Huber, P. Clinical and future applications of high intensity focused ultrasound in cancer. *Cancer Treat. Rev.* **2012**, *38*, 346−353.

(11) Marin, A.; Sun, H.; Husseini, G. A.; Pitt, W. G.; Christensen, D. A.; Rapoport, N. Y. Drug delivery in pluronic micelles: Effect of high-frequency ultrasound on drug release from micelles and intracellular uptake. *J. Controlled Release* **2002**, *84*, 39−47.

(12) Rwei, A. Y.; Paris, J. L.; Wang, B.; Wang, W.; Axon, C. D.; Vallet-Regí, M.; Langer, R.; Kohane, D. S. Ultrasound-triggered local anaesthesia. *Nat. Biomed Eng.* **2017**, *1*, 644−653.

(13) Tyler, W. J.; Tufail, Y.; Finsterwald, M.; Tauchmann, M. L.; Olson, E. J.; Majestic, C. Remote excitation of neuronal circuits using low-intensity, low-frequency ultrasound. *PLoS One* **2008**, *3*, No. e3511.

(14) Kim, H.; Chiu, A.; Lee, S. D.; Fischer, K.; Yoo, S. S. Focused ultrasound-mediated non-invasive brain stimulation: Examination of sonication parameters. *Brain Stimul.* **2014**, *7*, 748−756.

(15) Szablowski, J. O.; Lee-Gosselin, A.; Lue, B.; Malounda, D.; Shapiro, M. G. Acoustically targeted chemogenetics for the non-invasive control of neural circuits. *Nat. Biomed Eng.* **2018**, *2*, 475−484.

(16) Kobayashi, M.; Mizumoto, T.; Shibuya, Y.; Enomoto, M.; Takeda, M. Fluorescence tomography in turbid media based on acousto-optic modulation imaging. *Appl. Phys. Lett.* **2006**, *89*, 181102.

(17) Wang, Y. M.; Judkewitz, B.; Dimarzio, C. A.; Yang, C. Deep-tissue focal fluorescence imaging with digitally time-reversed ultrasound-encoded light. *Nat. Commun.* **2012**, *3*, 928.

(18) Yuan, B. Ultrasound-modulated fluorescence based on a fluorophore-quencher-labeled microbubble system. *J. Biomed. Opt.* **2009**, *14*, No. 024043.

(19) Yuan, B.; Liu, Y.; Mehl, P. M.; Vignola, J. Microbubble-enhanced ultrasound-modulated fluorescence in a turbid medium. *Appl. Phys. Lett.* **2009**, *95*, 181113.

(20) Fan, X.; Yun, S. H. The potential of optofluidic biolasers. *Nat. Methods* **2014**, *11*, 141−147.

(21) Yang, S.; Wang, Y.; Sun, H. D. Advances and Prospects for Whispering Gallery Mode Microcavities. *Adv. Opt. Mater.* **2015**, *3*, 1136−1162.

(22) Cho, S.; Humar, M.; Martino, N.; Yun, S. H. Laser particle stimulated emission microscopy. *Phys. Rev. Lett.* **2016**, *117*, 1−5.

(23) Chen, Q.; Zhang, X.; Sun, Y.; Ritt, M.; Sivaramakrishnan, S.; Fan, X. Highly sensitive fluorescent protein FRET detection using optofluidic lasers. *Lab Chip* **2013**, *13*, 2679−2681.

(24) Wu, X.; Oo, M. K. K.; Reddy, K.; Chen, Q.; Sun, Y.; Fan, X. Optofluidic laser for dual-mode sensitive biomolecular detection with a large dynamic range. *Nat. Commun.* **2014**, *5*, 1−7.

(25) Chen, Q.; Ritt, M.; Sivaramakrishnan, S.; Sun, Y.; Fan, X. Optofluidic lasers with a single molecular layer of gain. *Lab Chip* **2014**, *14*, 4590−4595.

(26) Polson, R. C.; Vardeny, Z. V. Cancerous tissue mapping from random lasing emission spectra. *J. Opt.* **2010**, *12*, No. 024010.

(27) Wang, Y.; Duan, Z.; Qiu, Z.; Zhang, P.; Wu, J.; Dingke, A.; Xiang, T. Random lasing in human tissues embedded with organic dyes for cancer diagnosis. *Sci. Rep.* **2017**, *7*, 1−7.

(28) Chen, Y. C.; Tan, X.; Sun, Q.; Chen, Q.; Wang, W.; Fan, X. Laser-emission imaging of nuclear biomarkers for high-contrast cancer screening and immunodiagnosis. *Nat. Biomed Eng.* **2017**, *1*, 724−735.

(29) Chen, Y. C.; Chen, Q.; Wu, X.; Tan, X.; Wang, J.; Fan, X. A robust tissue laser platform for analysis of formalin-fixed paraffin-embedded biopsies. *Lab Chip* **2018**, *18*, 1057−1065.

(30) Humar, M.; Yun, S. H. Intracellular microlasers. *Nat. Photonics* **2015**, *9*, 572−576.

(31) Schubert, M.; Steude, A.; Liehm, P.; Kronenberg, N. M.; Karl, M.; Campbell, E. C.; Powis, S. J.; Gather, M. C. Lasing within Live Cells Containing Intracellular Optical Microresonators for Barcode-Type Cell Tagging and Tracking. *Nano Lett.* **2015**, *15*, 5647−5652.

(32) Galanzha, E. I.; Weingold, R.; Nedosekin, D. A.; Sarimollaoglu, M.; Nolan, J.; Harrington, W.; Kuchyanov, A. S.; Parkhomenko, R. G.; Watanabe, F.; Nima, Z.; Biris, A. S.; Plekhanov, A. I.; Stockman, M. I.; Zharov, V. P. Spaser as a biological probe. *Nat. Commun.* **2017**, *8*, 15528.

(33) Wu, X.; Chen, Q.; Xu, P.; Chen, Y. C.; Wu, B.; Coleman, R. M.; Tong, L.; Fan, X. Nanowire lasers as intracellular probes. *Nanoscale* **2018**, *10*, 9729−9735.

(34) Fingas, M.; Fieldhouse, B.; Bobra, M. A.; Tennyson, E. The physics and chemistry of emulsions. In *Workshop on Emulsions*; Marine Spill Response Corporation, Washington, D.C., 1993; p 770.

(35) Mekis, A.; Nöckel, J. U.; Chen, G.; Stone, A. D.; Chang, R. K. Ray chaos and Q spoiling in lasing droplets. *Phys. Rev. Lett.* **1995**, *75*, 2682−2685.

(36) Nockel, J. U.; Stone, A. D. Chaotic light: a theory of asymmetric resonant cavities. *Adv. Ser. Appl. Phys.* **1996**, *3*, 389−426.

(37) Nöckel, J. U.; Stone, A. D. Ray and wave chaos in asymmertric resonant optical cavities. *Nature* **1997**, *385*, 45.

(38) Baryshnikov, Y.; Heider, P.; Parz, W.; Zharnitsky, V. Whispering gallery modes inside asymmetric resonant cavities. *Phys. Rev. Lett.* **2004**, *93*, 1−4.

(39) Ge, L.; Malik, O.; Türeci, H. E. Enhancement of laser power-efficiency by control of spatial hole burning interactions. *Nat. Photonics* **2014**, *8*, 871−875.

(40) Wu, J.; Du, G. Acoustic radiation force on a small compressible sphere in a focused beam. *J. Acoust. Soc. Am.* **1990**, *87*, 997−1003.

(41) Gmachl, C.; Capasso, F.; Narimanov, E. E.; Nöckel, J. U.; Stone, A. D.; Faist, J.; Sivco, D. L.; Cho, A. Y. High-power directional emission from microlasers with chaotic resonators. *Science* **1998**, *280*, 1556−1564.

(42) Gmachl, C.; Capasso, F.; Baillargeon, J. N.; Cho, A. Y. Kolmogorov−Arnold−Moser transition and laser action on scar modes in semiconductor diode lasers with deformed resonators. *Opt. Lett.* **2002**, *27*, 824−826.